

Low Thermal Conductivity in Franckeite Heterostructures

Jean Spiece,[†] Sara Sangtarash,[‡] Marta Mucientes,[†] Aday J. Molina-Mendoza,[¶]
Kunal Lulla,[†] Thomas Mueller,[¶] Oleg Kolosov,^{*,†} Hatef Sadeghi,^{*,‡} and
Charalambos Evangelidis,^{*,§,†}

[†]*Physics Department, Lancaster University, Lancaster LA1 4YW, United Kingdom*

[‡]*Device Modelling Group, School of Engineering, University of Warwick, CV4 7AL
Coventry, United Kingdom*

[¶]*Vienna University of Technology, Gusshausstrasse 27-29, Vienna A-1040, Austria*

[§]*Department of Materials, University of Oxford, Oxford OX1 3PH, United Kingdom*

E-mail: o.kolosov@lancaster.ac.uk; Hatef.Sadeghi@warwick.ac.uk;

charalambos.evangelidis@materials.ox.ac.uk

Abstract

Layered crystals are known to be good candidates for bulk thermoelectric applications as they open new ways to realise highly efficient devices. Two dimensional materials, isolated from layered materials, and their stacking into heterostructures have attracted intense research attention for nanoscale applications due to their high Seebeck coefficient and possibilities to engineer their thermoelectric properties. However, integration to thermoelectric devices is problematic due to their usually high thermal conductivities. Reporting on thermal transport studies between 150 and 300K, we demonstrate here, that franckeite, a naturally occurring 2D heterostructure, is a promising candidate for low dimensional thermoelectric applications. We find cross- and in-plane

thermal conductivity values at room temperature of 0.70 and $0.88\text{Wm}^{-1}\text{K}^{-1}$, respectively, which is the lowest value reported today for 2D-materials. Amazingly, a 1nm thick franckeite shows very low thermal conductivity similar to one of the most widely used thermoelectric material Bi_2Te_3 with the thickness of $10\text{-}20\text{nm}$. We show that this is due to the low Debye frequency of franckeite, a gap in its phonon band structure and scattering of phonon transport through van der Waals interface between different layers. This observation opens new routes for high efficient ultra-thin thermoelectric applications.

Introduction

Thermoelectric materials are of great interest, due to their ability to fabricate devices which convert the waste heat into electricity. Efficient thermoelectric devices require tuning of the materials Seebeck coefficient, electrical and thermal conductivity. The efficiency of a thermoelectric material is given by the thermoelectric figure of merit, $ZT = (\sigma S^2 T)/k$, and is proportional to the square of Seebeck coefficient S and electrical conductivity σ and inversely proportional to the thermal conductivity k .¹ Therefore, materials combining high S and σ and low k , which are generally rare, are ideal candidates for such devices. Many strategies have been applied to decrease the k without affecting the σ including creation of structural disorders, synthesizing materials with complex crystal structures, and use of organic-hybrid materials or low-dimensional nano-structured materials.²

Layered crystals are known to be good candidates for integration in thermoelectric applications,³ such as the Bi_2Te_3 -alloys which are among the best performing thermoelectric materials. Exfoliating such crystals, resulting in two dimensional (2D) materials, provide great opportunities to challenge commercially used materials as they offer the unique possibility of engineering their thermal conductivity.⁴ By stacking different 2D materials to create van der Waals (vdW) heterostructures, the phonon mismatch between the layers can be controlled and with the right assembly the thermal conductivity is reduced. Strategies

like stacking Bi_2Te_3 exfoliated thin films to form 'pseudosuperlattice',^{5,6} stacking graphene and MoS_2 monolayers^{7,8} or inserting different intercalants such as SnS and BiS in to TiS_2 vdW gap and creation of superlattices^{9,10} have been successful to decrease the thermal conductivity.

Instead of attempting the often very demanding 2D materials stacking, another strategy consists in using nature's ability of creating heterostructures. In contrast to a fabricated 2D-heterostructure, a natural one do not have any issues such as alignment or trapped residues in between the layers, which might cause uncontrolled change of the thermal or electrical resistance. Franckeite is such a material consisting of stacks of SnS_2 - like pseudo-hexagonal (H) and PbS - like pseudo-tetragonal (Q) layers (see Figure 1a) which can be isolated by liquid or air exfoliation^{11,12}. It demonstrates high electrical conductance with a narrow bandgap of $0.5 - 0.7\text{eV}$ and a Seebeck coefficient of $264\mu\text{V/K}$ at room temperature¹² which makes it an attractive candidate for realization of novel thermoelectric devices.

Here, we demonstrate that franckeite is a very promising candidate for thermoelectric applications. We study the thermal transport properties of thin flakes at various temperatures starting from 150K up to room temperature with Scanning Thermal Microscopy (SThM). We show that Franckeite H+Q layer has a very low in-plane and cross-plane thermal conductivity compared to other exfoliated or ultra-thin-film materials. This is supported by our Density Functional Theory (DFT) calculations that reveals that Franckeite has a low Debye frequency and therefore has low thermal conductivity.

Results and discussion

Figure 1a shows the molecular structure of layered franckeite. Our calculation using first principle simulations shows that the Debye frequency of franckeite is about $\hbar\omega = 40\text{meV}$. This means that franckeite is a soft material as confirmed by our Ultrasonic Force Microscopy study (See Supporting Information note 2) and can potentially possess a low thermal conduc-

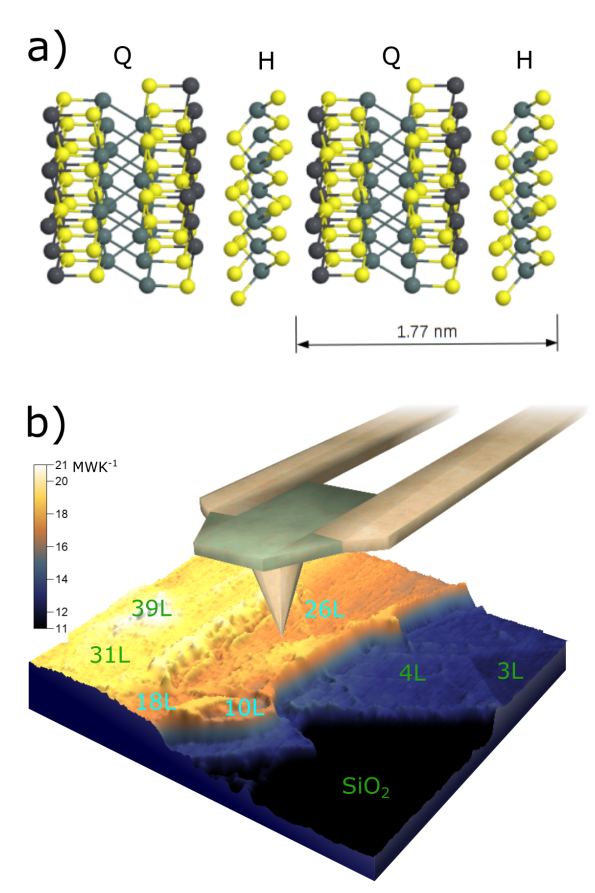


Figure 1: (a) Crystal structure of Franckeite. (b) Schematic representation of the SThM measurement, with 3D thermal resistance image at $T_{\text{sample}} = 156\text{K}$. Number of layers for the different areas are shown on the image (scan dimensions 55 μm).

tivity. Motivated by this observation, we isolated franckeite flakes on 280nm SiO₂ on Si by mechanical exfoliation (see Methods), resulting in areas of various thicknesses. We thermally characterise the sample by means of high vacuum SThM¹³ at sample temperatures varying from 150K – 300K as described elsewhere.⁷ Briefly, at each sample temperature, we thermally image the sample and record approach-retract SThM cycles. The tip-sample thermal contact resistance, R_X , for each pixel of the thermal image is obtained from the in-contact SThM image and the out-of-contact SThM signal from the approach-retract curve. Figure 1b shows a 3D representation of the thermal resistance image acquired at $T_{\text{sample}} = 156\text{K}$. Areas with thicknesses varying from 5 to 66 nm can be identified from the topography image (see Supporting Information note 1). Considering a H+Q layer thickness of about 1.7nm,¹²

we can identify areas consisting of 3, 4, 10, 26, 31, 39 of H+Q layers. The flakes' thermal resistance is higher than the one of Si/SiO₂ substrate and increases with the thickness.

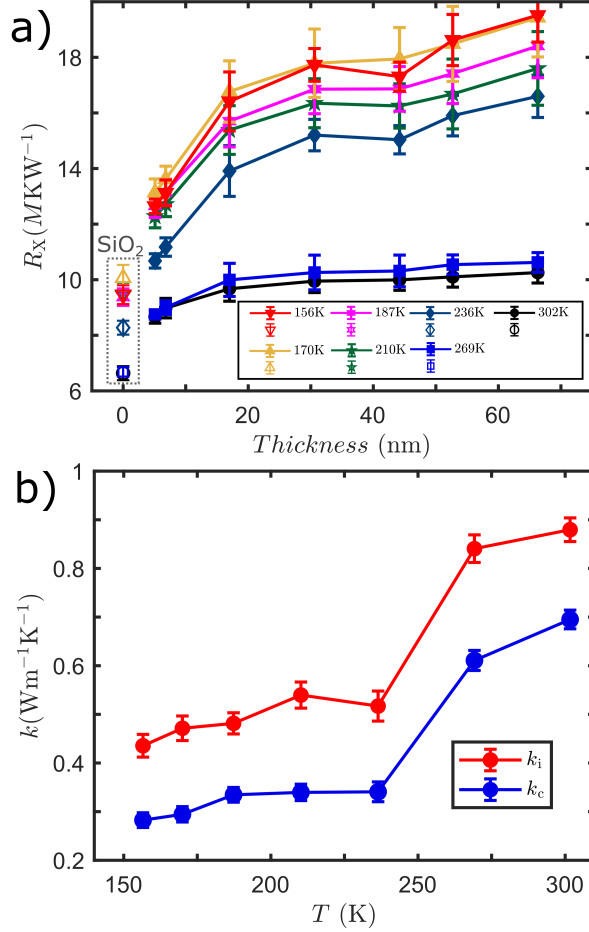


Figure 2: (a) Thermal Resistance R_X as a function of temperature for areas of different thicknesses (b) In-plane k_i and cross-plane k_c thermal conductivity of franckeite H+Q flake of 1.7nm thickness.

We extracted the average mean thermal resistance for each area and plotted it as a function of thickness at various temperatures (see Figure 2b). R_X increases with a high rate for the first 10 layers and then at room temperature almost saturates, implying that after a certain thickness, we are probing the thermal resistance of bulk franckeite. The increasing resistance with thickness trend is expected for layers with lower or comparable to the substrate thermal conductivity because they act as extra resistive interfaces for the heat flow to the substrate heat sink. For highly thermally conductive layers, such as graphene,

the trend is opposite^{14,15} because they act as extra heat transfer channels. The thermal resistance evolution with thickness could be a purely thickness dependent effect, related with thermal conductivity variation or substrate effects. In general the thermal conductivity of 2D materials is also affected when they are placed on a substrate due to change in the phonon dispersion and increase of the phonon scattering rate.^{14,16,17}

Regarding the temperature dependence, R_X for all thicknesses decreases with temperature, with the higher rate being for the thicker areas. For thinner areas (less than 10 layers), R_X is dominated by the thermal resistance of SiO_2 as revealed by the similar to SiO_2 thermal resistance (R_{X-S}) trend with temperature (see also Supporting Information note 1). In contrast, for thicker areas, R_X decreases in a different manner than R_{X-S} . The R_X saturation with temperature for thicker franckeite (more than 10 layers) is different than the SiO_2 trend. This observation implies that for such thicknesses, SThM is more sensitive to the material rather than the substrate properties.

To quantify the thermal conductivity of a single franckeite H+Q layer we assume diffusive thermal transport and thickness independent thermal conductivity. Franckeite, in contrast to other 2D materials, has a complex structure consisting of heavy atoms which is likely leading to a diffusive thermal transport mechanism.¹⁸ For such structures of low thermal conductivity it is not evident that thermal conductivity is strongly influenced by the number of layer.¹⁶ Under these assumptions we express the thermal SThM measured resistance as a sum of resistances: $R_X = R_t + R_{\text{int}} + R_s$, where R_t is the SThM tip thermal resistance, R_{int} the tip-franckeite thermal boundary resistance and R_s is the sample spreading resistance. R_t and R_{int} are not thickness-dependent and they remain constant for the different sample areas. With the use of a diffusive thermal transport model for layered material on a substrate, we express R_s as a function of the layer thickness and the thermal conductivities of the substrate and the material.^{15,19-21} By fitting the data for each temperature we extract the cross-plane (k_c) and in-plane (k_i) thermal conductivity (see Methods and SI for more details on the modeling and fitting procedure).

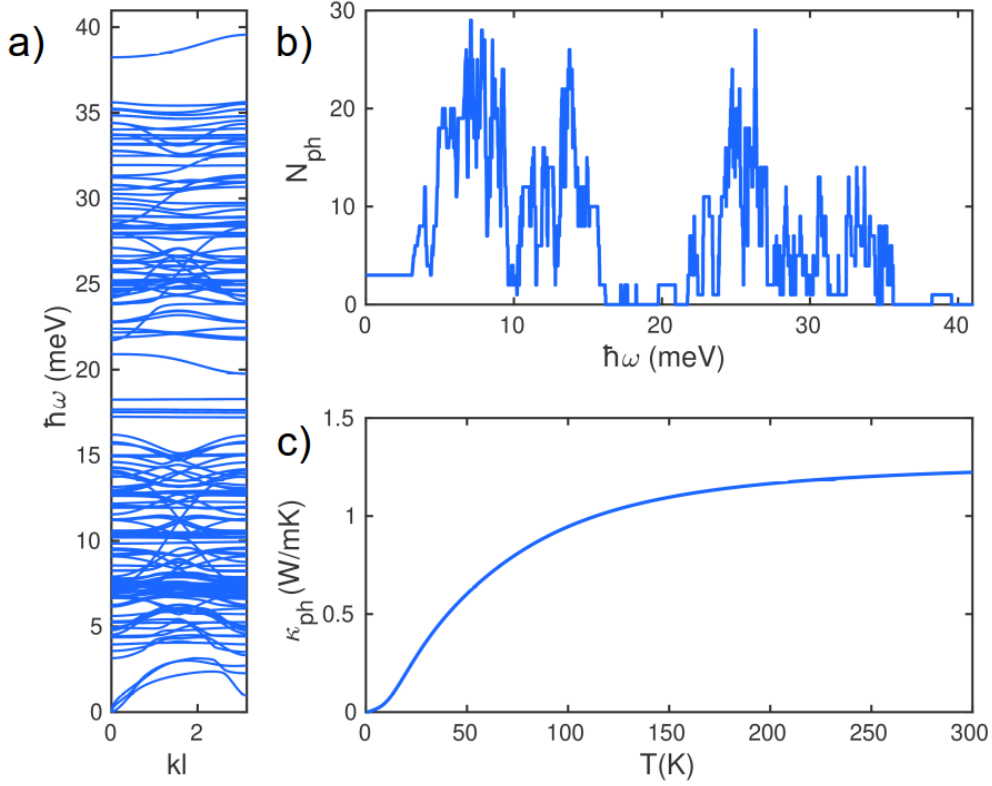


Figure 3: (a) Phonon band-structure of franckeite with the lattice structure shown in Fig 1b. (b) Number of open phonon conduction channel and (c) phonon contribution to thermal conductivity

In Figure 2b, k_c and k_i are plotted for each temperature. Both k_c and k_i are found to increase with temperature from 0.28 and $0.44\text{Wm}^{-1}\text{K}^{-1}$ at 156K to 0.70 and $0.88\text{Wm}^{-1}\text{K}^{-1}$ at room temperature, respectively. The thermal conductivity increase rate is much higher for temperatures higher than 240K. The anisotropy has a small decrease with temperature, which is possibly related with the activation of some phonon modes with temperature (see also Supplementary note 4).

To understand the physical mechanisms behind the thermal conductivity values and trends, we calculate the phonon band structure of franckeite (see Figure 3a) using density functional theory (see computational methods). From the band structure, we calculate the number of open phonon conduction channels in franckeite (Figure 3b) and its intrinsic

thermal conductivity (Figure 3 c). Our calculation shows that there are multiple open phonon channels between $0 - 16\text{meV}$ and $20 - 36\text{meV}$ but there are very few between $16 - 20\text{meV}$ due to a gap in phonon band structure. This gap and relatively low Debye frequency of franckeite leads to a calculated cross-plane thermal conductivity of $\sim 1.2\text{Wm}^{-1}\text{K}^{-1}$ at room temperature. This is the intrinsic thermal conductivity of franckeite (upper bound thermal conductivity) because in the calculations, we do not take scattering at the interfaces between electrodes and franckeite layers into account.

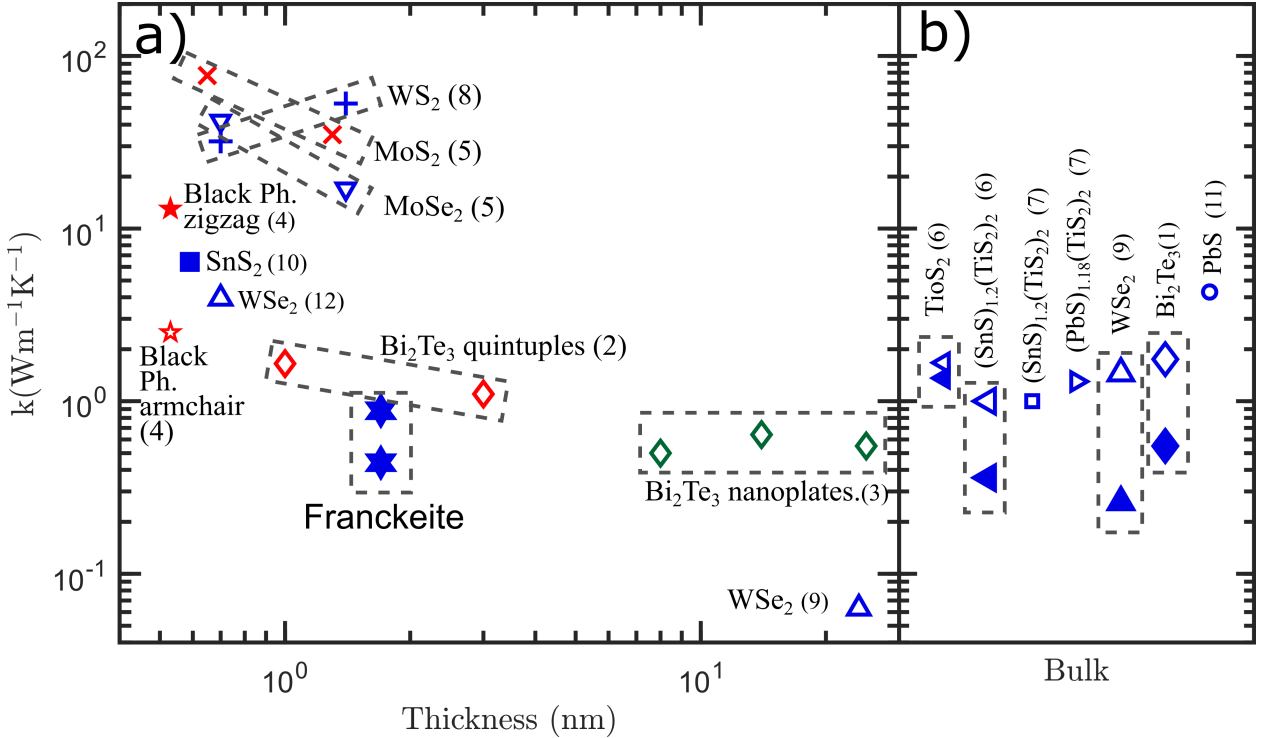


Figure 4: (a,b) Reported thermal conductivity values of layered materials with thickness (a) and of bulk layered materials (b). Note that, at (b) when two values for the same material are shown they correspond to cross- (filled) and in- (non-filled) plane values. The data come from: (1),⁵ (2),⁶ (3),²² (4),²³ (5),²⁴ (6),⁹ (7),¹⁰ (8),²⁵ (9),²⁶ (10),²⁷ (11),²⁸ (12)²⁹

The k_c and k_i values at room temperature are the the lowest values reported up to date for materials with similar thickness including mono- or few-layers of exfoliated materials or ultra-thin films suitable for thermoelectric applications. Figure 4 shows thermal conductivity values of typical layered thermoelectric materials with thickness in addition to some bulk-materials values. An H+Q franckeite layer has the lowest in-plane and cross-plane

thermal conductivities compared to all other materials with similar thickness. Amazingly, the thermal conductivity of a 1nm thick H+Q franckeite is similar to that of reported for Bi_2Te_3 but with a thickness of 10-20nm as measured or calculated theoretically. Thermal conductivity of a H+Q franckeite is two orders of magnitude lower than WS_2 with this ratio even larger for MoS_2 which is having very high Seebeck coefficient however, being unsuitable for thermoelectrics due to its high thermal conductivity. It is almost an order of magnitude lower than black phosphorous which has similar Seebeck coefficient as franckeite and just one order of magnitude higher than WSe_2 which is the lowest thermal conductivity continuous material. Furthermore, franckeite's thermal conductivity is smaller than most bulk layered materials with inserted different intercalants in the vdW gap designed for thermoelectric applications such as $(\text{SnS})_{1.2}(\text{TiS}_2)_2$, $(\text{PbS})_{1.18}(\text{TiS}_2)_2$, $(\text{BiS})_{1.2}(\text{TiS}_2)_2$ and $(\text{SnS})_{1.2}(\text{TiS}_2)_2$. The intercalation method has as a result the creation of superlattices and the decrease of the thermal conductivity of the initial material due to suppressed phonon transport caused by weaker interlayer bonding.⁹ In the case of franckeite which has a natural superlattice is interesting to see the relation between the H+Q layers thermal conductivity and H layer itself. The thermal conductivity of SnS_2 layer (H layer of franckeite), is almost an order of magnitude higher than the H+Q layers together. This is because of the additional phonon scattering at the interface³⁰ between H and Q layers and through Q layer as demonstrated using a tight-binding model in the supporting information note 4.

Conclusion

In summary, with a combined experimental and theoretical study the thermal properties of franckeite natural heterostructure in the nano-scale, for temperatures ranging from 150 to 300K were studied. In-plane and cross-plane thermal conductivity range from 0.28 and $0.44\text{Wm}^{-1}\text{K}^{-1}$ at 156K to 0.70 and $0.88\text{Wm}^{-1}\text{K}^{-1}$, respectively at room temperature. We showed that the low thermal conductivity values are due to the a gap in phonon band structure, the low Debye frequency and the additional phonon scattering at the interface

between H and Q layers of franckeite. These values which are among the lowest reported for 2D materials and ultra-thin-films, that in combination to the high electrical conductivity and Seebeck coefficient make franckeite a promising candidate for integration to micro-scale thermoelectric applications at room temperature.

Methods

Experimental Methods

Sample fabrication: Few-layer franckeite flakes are exfoliated from bulk material and transferred on a SiO₂ substrate thermally grown on a Si wafer. The bulk franckeite material (San Jose Mine, Oruro City, Bolivia) is first scratched with a scalpel on an adhesive tape, resulting in thin chips of material. These chips are then thinned-down by repeatedly bringing the tape in contact with itself and peeling it off. Once a significant amount of thin material is obtained, a polydimethylsiloxane (PDMS) stamp is used to exfoliate franckeite from the adhesive tape. Transmission-mode optical microscopy is then employed to identify the thin flakes prior transfer on the SiO₂/Si substrate (as described by Castellanos-Gomez et al.³¹).

Thermal Spreading Resistance model: We express the thermal SThM measured resistance as a sum of resistances: $R_X = R_t + R_{\text{int}} + R_s$, where R_t is the SThM tip thermal resistance, R_{int} the tip-franckeite thermal boundary resistance and R_s is the sample spreading resistance. We estimate R_t out of the franckeite free SiO₂ area (see SI) and express R_{int} as $R_{\text{int}}/\pi\rho^2$, where R_{int} is the SiO₂-franckeite interface thermal resistivity and ρ is the tip radius which we obtained from the thermal images and SEM imaging of the SThM tip (see Supporting Information note 1). R_s of a layered material on a substrate is expressed as a function of the layer thickness and the thermal conductivities of the substrate and the material.^{15,19–21} Since the thermal conductivity of SiO₂ is known,³² R_X is determined by the only remaining unknowns: k_{\parallel} and R_{int} . We also account for thermal transport anisotropy and we define k_c and k_i for the cross-plane and in-plane thermal conductivity, respectively.

For very thin areas (10 layers) compared to the tip diameter (80nm), the heat flow from the tip to the substrate is almost vertical³³ and we use an isotropic model with $k_{\parallel} = k_c$ and r_{int} as fitting parameters. For thicker areas this assumption is not valid and we use an orthotropic model considering both k_c and k_{\parallel} (see Methods and Supporting Information note 3 for more details on the modeling procedure).

Computational Methods

Geometry optimization: The geometry optimisation of franckeite unit cell was performed using the SIESTA implementation of density functional theory (DFT), to the force tolerance of 10 meV/Å with a double-polarized basis set (DZP) and the Generalized Gradient Approximation (GGA) functional with Perdew-Burke-Ernzerhof (PBE) parameterization. A real-space grid was defined with an equivalent energy cut-off of 350 Ry.

Phonon dispersion relation: From the optimised unit cell geometry of franckeite, we construct a super-cell shown in figure 1a and construct dynamical matrix as described below for each super-cell (k_0) as well as coupling matrix elements (K_1) to the neighbouring cell in H/Q/H/Q configuration (see Figure 1 a). We then calculate phonon dispersion relation using these k_0 and k_1 and the method described in³⁴

Phonons transport and thermal conductivity: Following the method described in^{34 35 30} each atom was displaced from the relaxed optimised position in the positive and negative x, y and z directions with 0.01Å . For each displacement, the forces F in three directions on all atoms were then calculated and used to construct the dynamical matrix $D=K/M$ where the mass matrix M and Hessian matrix K obtained from finite differences. To satisfy momentum conservation, the diagonal terms in K is calculated by negative of sum of off-diagonal terms. The phonon transmission then can be calculated from the relation $T_p = \text{Trace}(\Gamma_L(\omega)G(\omega)\Gamma_R(\omega)G^\dagger(\omega))$ where $\Gamma_{L,R} = i(\sum_{L,R}(\omega) - \sum_{L,R}^\dagger(\omega))$ describes the level broadening due to the coupling to the left L and right R electrodes, $\sum_{L,R}(\omega)$ are the retarded self-frequencies associated with this coupling and $G = (\omega^2 I - D - \sum_L - \sum_R)^{-1}$

is the retarded Green's function, where D and I are the dynamical and the unit matrices, respectively. The phonon thermal conductivity κ_p at temperature T is then calculated from $\kappa_p(T) = \hbar/2\pi \int_0^\infty \omega T_p(\omega)(\partial f/\partial T)$ where $f = 1/(e^{\hbar\omega/k_B T} - 1)$ is Bose–Einstein distribution function and \hbar and k_B are reduced Planck's and Boltzmann's constants, respectively.

Acknowledgement

H.S. acknowledges the UKRI for Future Leaders Fellowship number MR/S015329/2. S.S. acknowledges the Leverhulme Trust for Early Career Fellowship no. ECF-2018-375. O.K., C.E., and J.S. acknowledge the support of the EU grant QUANTIHEAT (project 604668). O.K. acknowledges core 3 Graphene Flagship EU project and EP/v00767XII EPSRC grant.

Conflicts of interest

There are no conflicts to declare.

Data Availability

The input files to reproduce simulation data can be found at: <https://warwick.ac.uk/nanolab>

References

- (1) Biswas, K.; He, J.; Blum, I. D.; Wu, C.-I.; Hogan, T. P.; Seidman, D. N.; Draavid, V. P.; Kanatzidis, M. G. High-performance bulk thermoelectrics with all-scale hierarchical architectures. *Nature* **2012**, *489*, 414–418.
- (2) Yin, Y.; Baskaran, K.; Tiwari, A. A Review of Strategies for Developing Promising Thermoelectric Materials by Controlling Thermal Conduction. *physica status solidi (a)* **2019**, *216*, 1800904.

- (3) Samanta, M.; Ghosh, T.; Chandra, S.; Biswas, K. Layered Materials with 2D Connectivity for Thermoelectric Energy Conversion. *Journal of Materials Chemistry A* **2020**,
- (4) Ahn, E. C.; Wong, H.-S. P.; Pop, E. Carbon nanomaterials for non-volatile memories. *Nature Reviews Materials* **2018**, *3*, 1–15.
- (5) Teweldebrhan, D.; Goyal, V.; Balandin, A. A. Exfoliation and characterization of bismuth telluride atomic quintuples and quasi-two-dimensional crystals. *Nano letters* **2010**, *10*, 1209–1218.
- (6) Qiu, B.; Ruan, X. Thermal conductivity prediction and analysis of few-quintuple Bi₂Te₃ thin films: A molecular dynamics study. *Applied physics letters* **2010**, *97*, 183107.
- (7) Evangeli, C.; Spiece, J.; Sangtarash, S.; Molina-Mendoza, A. J.; Mucientes, M.; Mueller, T.; Lambert, C.; Sadeghi, H.; Kolosov, O. Nanoscale Thermal Transport in 2D Nanostructures from Cryogenic to Room Temperature. *Advanced Electronic Materials* **2019**, *5*, 1900331.
- (8) Sadeghi, H.; Sangtarash, S.; Lambert, C. J. Cross-plane enhanced thermoelectricity and phonon suppression in graphene/MoS₂ van der Waals heterostructures. *2D Materials* **2016**, *4*, 015012.
- (9) Wan, C.; Wang, Y.; Wang, N.; Norimatsu, W.; Kusunoki, M.; Koumoto, K. Intercalation: Building a natural superlattice for better thermoelectric performance in layered chalcogenides. *Journal of electronic materials* **2011**, *40*, 1271–1280.
- (10) Wan, C.; Wang, Y.; Wang, N.; Koumoto, K. Low-thermal-conductivity (MS)_{1+x}(TiS₂)₂ (M= Pb, Bi, Sn) misfit layer compounds for bulk thermoelectric materials. *Materials* **2010**, *3*, 2606–2617.
- (11) Velický, M.; Toth, P. S.; Rakowski, A. M.; Rooney, A. P.; Kozikov, A.; Woods, C. R.; Mishchenko, A.; Fumagalli, L.; Yin, J.; Zólyomi, V., et al. Exfoliation of natural van der

- Waals heterostructures to a single unit cell thickness. *Nature communications* **2017**, *8*, 1–11.
- (12) Molina-Mendoza, A. J.; Giovanelli, E.; Paz, W. S.; Niño, M. A.; Island, J. O.; Evangelini, C.; Aballe, L.; Foerster, M.; Van Der Zant, H. S.; Rubio-Bollinger, G., et al. Franckeite as a naturally occurring van der Waals heterostructure. *Nature communications* **2017**, *8*, 1–9.
- (13) Gomès, S.; Assy, A.; Chapuis, P.-O. Scanning thermal microscopy: A review. *physica status solidi (a)* **2015**, *212*, 477–494.
- (14) Pumarol, M. E.; Rosamond, M. C.; Tovee, P.; Petty, M. C.; Zeze, D. A.; Falko, V.; Kolosov, O. V. Direct nanoscale imaging of ballistic and diffusive thermal transport in graphene nanostructures. *Nano Letters* **2012**, *12*, 2906–2911.
- (15) Menges, F.; Riel, H.; Stemmer, A.; Dimitrakopoulos, C.; Gotsmann, B. Thermal transport into graphene through nanoscopic contacts. *Physical review letters* **2013**, *111*, 205901.
- (16) Gu, X.; Wei, Y.; Yin, X.; Li, B.; Yang, R. Colloquium: Phononic thermal properties of two-dimensional materials. *Reviews of Modern Physics* **2018**, *90*, 041002.
- (17) Balandin, A. A. Thermal properties of graphene and nanostructured carbon materials. *Nature materials* **2011**, *10*, 569–581.
- (18) Shen, M.; Keblinski, P. Ballistic vs. diffusive heat transfer across nanoscopic films of layered crystals. *Journal of Applied Physics* **2014**, *115*, 144310.
- (19) Yovanovich, M. M.; Culham, J. R.; Teertstra, P. Analytical modeling of spreading resistance in flux tubes, half spaces, and compound disks. *IEEE Transactions on Components, Packaging, and Manufacturing Technology: Part A* **1998**, *21*, 168–176.

- (20) Hwang, G.; Kwon, O. Measuring the size dependence of thermal conductivity of suspended graphene disks using null-point scanning thermal microscopy. *Nanoscale* **2016**, *8*, 5280–5290.
- (21) Sadeghi, M. M.; Park, S.; Huang, Y.; Akinwande, D.; Yao, Z.; Murthy, J.; Shi, L. Quantitative scanning thermal microscopy of graphene devices on flexible polyimide substrates. *Journal of Applied Physics* **2016**, *119*, 235101.
- (22) Pettes, M. T.; Maassen, J.; Jo, I.; Lundstrom, M. S.; Shi, L. Effects of surface band bending and scattering on thermoelectric transport in suspended bismuth telluride nanoplates. *Nano letters* **2013**, *13*, 5316–5322.
- (23) Chen, J.; Chen, S.; Gao, Y. Anisotropy enhancement of thermal energy transport in supported black phosphorene. *The journal of physical chemistry letters* **2016**, *7*, 2518–2523.
- (24) Zhang, X.; Sun, D.; Li, Y.; Lee, G.-H.; Cui, X.; Chenet, D.; You, Y.; Heinz, T. F.; Hone, J. C. Measurement of lateral and interfacial thermal conductivity of single- and bilayer MoS₂ and MoSe₂ using refined optothermal Raman technique. *ACS applied materials & interfaces* **2015**, *7*, 25923–25929.
- (25) Peimyoo, N.; Shang, J.; Yang, W.; Wang, Y.; Cong, C.; Yu, T. Thermal conductivity determination of suspended mono- and bilayer WS₂ by Raman spectroscopy. *Nano Research* **2015**, *8*, 1210–1221.
- (26) Chiritescu, C.; Cahill, D. G.; Nguyen, N.; Johnson, D.; Bodapati, A.; Koblinski, P.; Zschack, P. Ultralow thermal conductivity in disordered, layered WSe₂ crystals. *Science* **2007**, *315*, 351–353.
- (27) Shafique, A.; Samad, A.; Shin, Y.-H. Ultra low lattice thermal conductivity and high carrier mobility of monolayer SnS₂ and SnSe₂: a first principles study. *Physical Chemistry Chemical Physics* **2017**, *19*, 20677–20683.

- (28) Zhang, Y.; Ke, X.; Chen, C.; Yang, J.; Kent, P. Thermodynamic properties of PbTe, PbSe, and PbS: First-principles study. *Physical review B* **2009**, *80*, 024304.
- (29) Zhou, W.-X.; Chen, K.-Q. First-principles determination of ultralow thermal conductivity of monolayer WSe₂. *Scientific reports* **2015**, *5*, 15070.
- (30) Sadeghi, H.; Sangtarash, S.; Lambert, C. Cross-plane enhanced thermoelectricity and phonon suppression in graphene/MoS₂ van der Waals heterostructures. *2D Materials* **2016**, *4*, 015012.
- (31) Castellanos-Gomez, A.; Buscema, M.; Molenaar, R.; Singh, V.; Janssen, L.; Van Der Zant, H. S.; Steele, G. A. Deterministic transfer of two-dimensional materials by all-dry viscoelastic stamping. *2D Materials* **2014**, *1*, 011002.
- (32) Anis-ur Rehman, M.; Maqsood, A. Measurement of thermal transport properties with an improved transient plane source technique. *International journal of thermophysics* **2003**, *24*, 867–883.
- (33) Feser, J. P.; Cahill, D. G. Probing anisotropic heat transport using time-domain thermoreflectance with offset laser spots. *Review of Scientific Instruments* **2012**, *83*, 104901.
- (34) Sadeghi, H. Theory of Electron, Phonon and Spin Transport in Nanoscale Quantum Devices. *Nanotechnology* **2018**, *29*, 373001.
- (35) Ferrer, J.; et al., GOLLUM: a next-generation simulation tool for electron, thermal and spin transport. *New Journal of Physics* **2014**, *16*, 093029.